Preliminary human evaluation of MRI-guided transurethral ultrasound therapy for the treatment of localized prostate cancer

R. Chopra[1,2], M. Bronskill[1,2], M. Haider[3,4], and L. Klotz[5,6]

[1]Imaging Research, Sunnybrook Health Sciences Centre, Toronto, Ontario, Canada, [2]Medical Biophysics, University of Toronto, Toronto, Ontario, Canada, [3]Medical Imaging, Sunnybrook Health Sciences Centre, Toronto, Ontario, Canada, [4]Medical Imaging, University of Toronto, Toronto, Ontario, Canada, [5]Urology, Sunnybrook Health Sciences Centre, Toronto, Ontario, Canada, [6]Surgery, University of Toronto, Toronto, Ontario, Canada

Introduction

Minimally-invasive, image-guided treatments for localized prostate cancer offer a potential alternative to either active surveillance or radical treatments (surgery, radiation therapy). Integration with MRI can provide both disease targeting and therapy monitoring using the same modality. MRI-guided transurethral ultrasound therapy integrates high intensity ultrasound energy delivered from a transurethral device for thermal coagulation of prostate tissue with online control of treatment using MR thermometry [1]. This technology has been under development within our group for a number of years, and has been evaluated successfully in simulations [2], gel phantoms [3], and a preclinical canine model [4]. This study reports on the initial human experience using this technology as part of a preliminary clinical study of safety and feasibility in prostate cancer patients.

Methods

Men diagnosed with low- to intermediate- risk prostate cancer (T1/T2A, PSA<15 ng/ml, Gleason < 7 (3+4)) and scheduled for radical prostatectomy were enrolled into this study. Prior to surgery, subjects underwent treatment of a subvolume within the prostate gland with MRI-guided transurethral ultrasound therapy. Imaging was performed in a standard clinical 1.5T MR imager (Signa, GE Healthcare, USA) using an 8-channel cardiac phased array coil for imaging. Subjects were administered a spinal anesthetic to remove sensation and motor control of the pelvis and legs using techniques developed for brachytherapy. Following anesthesia, a transurethral device was inserted into the prostate gland and attached to an MRI-compatible positioning system which included a rotational motor. A fiber-optic temperature sensor was inserted into the rectum for core body temperature measurements. The subject was then transported into the MRI and advanced into the bore of the scanner. Preliminary images were acquired to measure the location of the ultrasound transducers within the prostate and adjustments were made as necessary. Oblique-axial T2-weighted images were acquired transverse to the device to select a region within the gland for treatment. High-intensity ultrasound energy was delivered to this region of the prostate, while MR images were acquired continuously every five seconds (FSPGR, FOV=26cm, 128x128, slice=10mm, TE=9ms, TR=40ms) and the spatial temperature distribution was calculated by phase subtraction using the PRF-shift method of thermometry. The temperature maps were analyzed during treatment by the delivery system, and the rate of rotation and output power of the ultrasound applicator were adjusted in order to elevate the temperature along the target boundary to 55°C. Ultrasound was delivered from a 10mm long by 3.5mm wide planar transducer operating at 8MHz, with an acoustic intensity up to 10W/cm2. After the completion of heating, contrast-enhanced images were acquired (3D FGRE, TE=min full, flip=13°, slice=2mm, 256x256, FOV=26cm) after intravenous injection of 0.1mmol/kg of Omniscan (GE Healthcare, USA). Once subjects emerged from the MRI, they were transported immediately to the OR for radical prostatectomy. The prostate was obtained and sectioned in the plane of imaging using techniques similar to those described previously [5], and the pattern of thermal damage observed on H&E stained whole-mount sections was compared with the imaging measurements obtained during treatment.

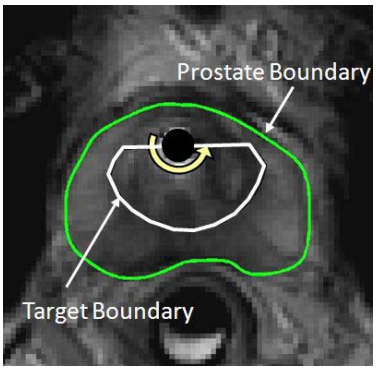

Figure 1: Target boundary selected for treatment

Results

The spinal anesthetic was well tolerated by all subjects, and enabled efficient insertion of the transurethral ultrasound applicator and subsequent attachment to the positioning system. The entire apparatus fitted within the 55-cm bore of the MRI and subjects remained stationary for the duration of treatment. The treatment lasted about two hours, including <10 minutes of actual ultrasound delivery. MR temperature measurements within the prostate gland were stable, and a temperature uncertainty of approximately 1.5°C was measured. A semicircular target boundary was chosen (Figure 1), with radii ranging from 10 to 18mm based on the prostate geometry and the treatment algorithm was developed for this particular ultrasound frequency. The maximum temperature distribution during treatment (Figure 2) depicted a continuous region of heating within the target boundary, and accurate heating of the outer boundary to the desired 55°C. The mean targeting error was less than 2 mm, which was on the order of 1 pixel in the thermometry images. The histological section obtained in the plane of treatment also depicted a continuous region of thermal damage that corresponded to the shape of the heating pattern (Figure 3). Post-treatment contrast-enhanced imaging revealed regions of non-enhancement within the target boundary, and signal enhancement extending 4-5mm beyond the boundary (Figure 3). The non-enhancing region was less well-defined than the pattern of thermal damage depicted on histology, and the spatial heating pattern measured with MR thermometry.

Conclusion

The results of this initial clinical study confirmed the capability of generating precise spatial heating patterns in the prostate gland using transurethral ultrasound therapy. In addition, the feasibility of using MR thermometry to control heating precisely in the prostate gland has been demonstrated in humans. These results motivate continued development of this technology for precise, minimally-invasive treatment of localized prostate cancer.

References

1. Chopra *et al*, Med Phys, 2008. 2. Burtnyk *et al*, Int J Hyperthermia, 2009. 3. Tang *et al*, Phys Med Biol, 2007. 4. Chopra *et al*, Phys Med Biol, 2009. 5. Boyes *et al*, J Urol, 2007

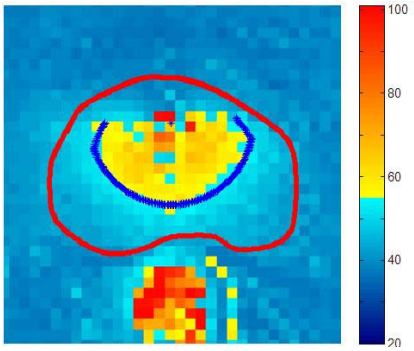

Figure 2: Maximum temperature distribution measured during treatment

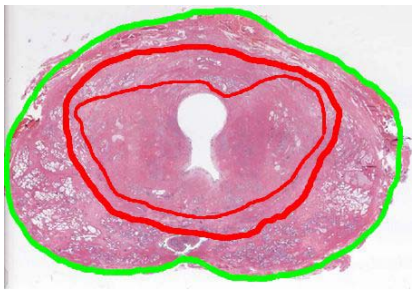

Figure 2: H&E stained section showing inner and outer boundary of thermal damage

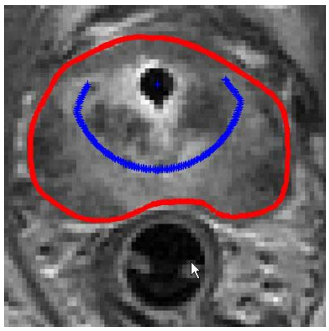

Figure 4: Contrast enhanced image obtained after treatment